Lab on a Chip

Accepted Manuscript

This is an *Accepted Manuscript*, which has been through the Royal Society of Chemistry peer review process and has been accepted for publication.

Accepted Manuscripts are published online shortly after acceptance, before technical editing, formatting and proof reading. Using this free service, authors can make their results available to the community, in citable form, before we publish the edited article. We will replace this *Accepted Manuscript* with the edited and formatted *Advance Article* as soon as it is available.

You can find more information about *Accepted Manuscripts* in the Information for Authors.

Please note that technical editing may introduce minor changes to the text and/or graphics, which may alter content. The journal's standard Terms & Conditions and the Ethical guidelines still apply. In no event shall the Royal Society of Chemistry be held responsible for any errors or omissions in this *Accepted Manuscript* or any consequences arising from the use of any information it contains.

ROYAL SOCIETY OF CHEMISTRY

www.rsc.org/loc

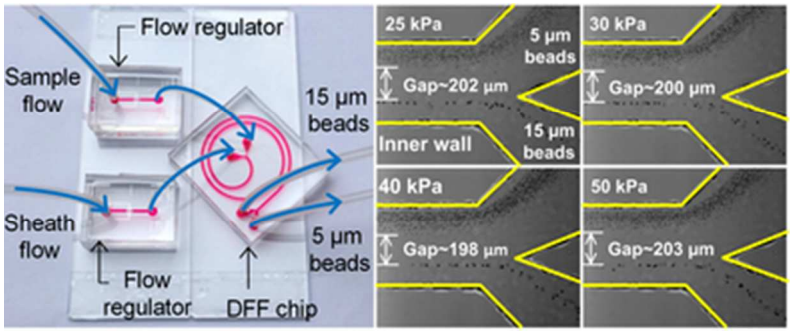

This paper presents a novel passive flow regulator for steady and high-throughtput inertial isolation of differently sized microbeads.
33x13mm (300 x 300 DPI)

Lab on a Chip Accepted Manuscript

Journal Name

RSCPublishing

ARTICLE

A passive flow regulator with low threshold pressure for high-throughput inertial isolation of microbeads†

Cite this: DOI: 10.1039/xoxxoooooox

Xinjie Zhang,§[a] Nan Xiang,§[a] Wenlai Tang,[a] Di Huang,[a] Xin Wang, [a] Hong Yi, [a] and Zhonghua Ni*[a]

Received ooth January 2012,
Accepted ooth January 2012

DOI: 10.1039/xoxxoooooox

www.rsc.org/

In this work, we present a novel passive flow regulator fabricated by stacking five functional layers. To understand the flow-rate regulation characteristics, a series of prototype devices with different structural dimensions are investigated. The experimental results show that our regulator can export a constant delivery flow-rate up to 4.38±0.1 ml/min with variations less than 5%, and the minimum threshold pressures for achieving constant flow-rate is only 10 kPa. As compared with previously reported regulators, our regulator offers a much wider flow-rate regulation range under lower threshold pressures. To validate the practical function of our regulator, a low pressure gas-driven flow system integrated with two passive flow regulators and a Dean flow fractionation chip is constructed to achieve high-throughput inertial isolation of differently sized microbeads. The isolation performance is found to be totally independent of inlet pressure, which permits the use of portable and low-cost flow-driving apparatuses for accurate flow control. Therefore, the passive flow regulator proposed in our work is potentially useful for the steady injection and accurate control of sample fluid in low cost, miniaturized microfluidic systems.

Introduction

In most microfluidic systems, sample injection and transportation need to be accurately controlled by peripheral equipment (e.g., syringe pumps)[1,2]. However, the high cost and bulky volume of these facilities prevent them from being integrated with lab-on-a-chip units, which hinders the propagation of microfluidic devices. Fortunately, with the recent development of soft lithography techniques, various types of micropumps[3-5] and microvalves[6-9] have been invented for driving or switching microfluids. Amongst these, microfluidic flow regulators have attracted increasing attention in recent years, and have potential applications in drug delivery systems (DDS)[10], point-of-care tests (POCT)[11] and integrated microfluidic systems[12] due to their advantage of accurate fluid control.

The microfluidic flow regulators from recent research fall into two categories, which are active ones and passive ones. Active flow regulators regulate the flow-rate in microchannels with the assistance of external units. For examples, the flow-rate can be easily regulated through pressurizing the control channel so as to change the dimension and resistance of the fluidic channels. The forces for pressurizing the control channel can be generated through the triggering of automated actuators[13], thermally actuated microfluidic relay valves[14], or adjusting the viscosity of fluids[15]. Due to the rapid response and accurate action of external units, active flow regulators can adjust flow-rate continuously in a high-throughput manner, and thus have been successfully employed for high-throughput particles/cells sorting[16,17]. However, the requirements of steady power sources, continuous fluid inputs, and extra external units limit the application of active flow regulators in integrated, low cost, and miniaturized microfluidic systems. Unlike the active ones, passive devices adjust the flow-rate automatically by changing the dimension of the fluidic channels without the assistant of external units or consuming energy. The working principles of the reported passive flow regulators are mainly dependent on the nonlinear relationship between flow-rate (Q) and gas pressure (P), that is, the flow-rate (Q) will be finally saturated with the increase of applied pressure (P). In recent research on passive flow regulators, the flow-rate was adjusted typically based on the elastic deflection of flexible membrane[18-21] or thin flap[22] under pressure variations. Due to the unique features of passive flow regulators, valuable applications have already been realized in fuel supply[23], fuel cell[24] and DDS[18]. Although many efforts have been made in previous works, improvements can still be made in both the structures and characteristics of the regulator so as to extend the toolbox for more practical applications. For example, a high delivery flow-rate is often required for applying the regulator to high-throughput particle/cell separations (e.g., inertial isolation).

In this work, we present a novel passive flow regulator which consists of five stacked polydimethylsiloxane (PDMS) layers. To understand the flow-rate characteristics of our regulator, a series of prototype devices with different structural dimensions are fabricated, and the influence of critical parameters (e.g., membrane length and cross-sectional dimensions) on flow-rate is systematically investigated. To probe into the practical function of our regulator, we construct a low-pressure gas-driven flow system consisted of two passive flow regulators and a Dean Flow Fractionation (DFF) chip, to achieve the high-throughput inertial isolation of microbeads.

Lab on a Chip Accepted Manuscript

Structure and principle

Fig. 1 illustrates the detailed structure of the proposed passive flow regulator which consists of two control channel layers, one main channel layer and two membranes. The upper and bottom layers comprise identical control channels which are used to induce the deformation of integrated membranes. The middle main channel layer holds an open straight channel containing a contraction near the middle region to define the original flow resistance of our regulator. The control channels and the main channel are respectively separated by two elastic membranes which can easily deform under the action of flow pressure. When assembling the individual layers, the control channels of the upper and bottom layers align to each other as illustrated in the enlarged image of the axonometric drawing in Fig. 1, forming two parallel membranes stretching across the contraction region of the main channel (see the section A-A view in Fig. 1). The proposed multilayer-stacked architecture in our work overcomes the aspect-ratio limitation of the previously reported parallel membrane valve in which large area of thin membrane is easily broken during the PDMS demolding process[21].

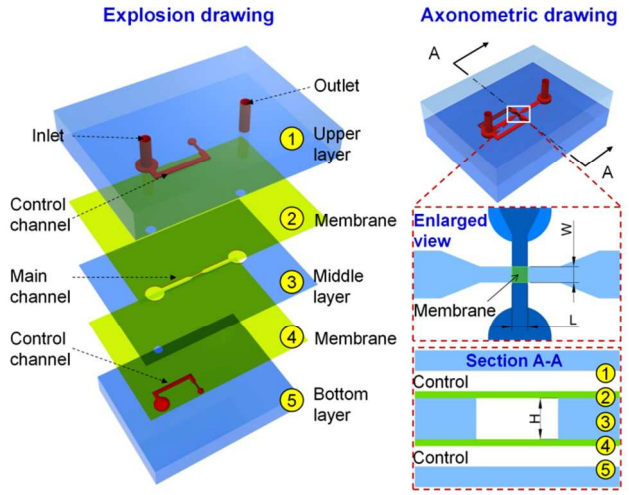

Fig. 1 Schematic diagram of our passive flow regulator. The left figure is the explosion drawing which shows the five-layer-stacked structure. The right figure shows the axonometric drawing, which includes an enlarged view and a cross-sectional view of crossed channels.

To demonstrate the working principle of our novel passive flow regulator, the nonlinear model of Fluid-Structure Interaction (FSI) was solved by using COMSOL Multiphysics®. Fig. 2 illustrates the numerical simulation results of the membrane deformation and the flow velocity near the crossed channel region after applying a pressure increment ΔP at the inlet. The parallel membranes will simultaneously deflect to each other under the pressure forces generated by the control channel, which results in the increase of the flow resistance of the main channel. The increased resistance compensates the pressure increment, making the flow-rate to reach a final constant Q_c after the inlet pressure is larger than a threshold value. As a comparison, we also simulated the flow-rate characteristics in a regulator without membranes. The obtained Q-P curve indicates that the flow-rate increases linearly with the increase of inlet pressure due to the nearly constant flow resistance.

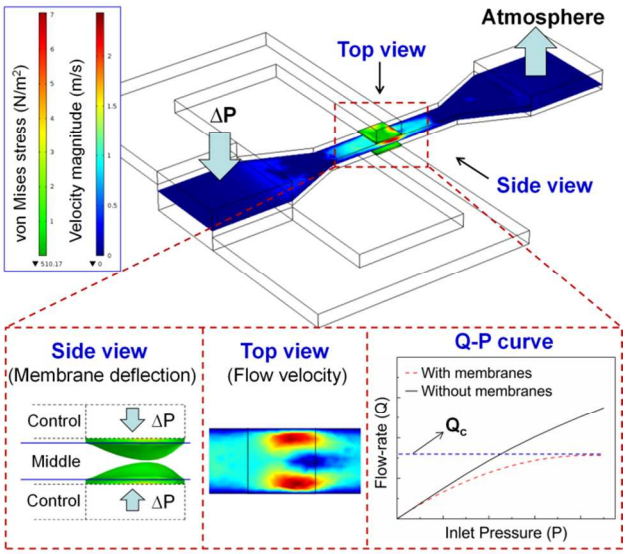

Fig. 2 Working principle of our passive flow regulator. The insets show the membrane deflection in side view, the flow velocity distribution in top view, and the Q-P curves obtained under the conditions with and without membranes.

Design and fabrication

Device design

Several types of prototype devices with different dimensions were designed to evaluate the functional performances of our passive flow regulators. Specifically, the height of the main channel (H) is set to be 75 μm or 130 μm, and the contraction gap width (W) is designed to be 100 μm or 200 μm. To minimize the resistance of the main channel, we set the width of the main channel to be 600 μm, which is much wider than that of the contraction gap. Therefore, the actual flow resistance of the main channel is determined by the H and W. The thicknesses of the two membranes are identical, both designed as 10 μm. The widths of the control channels in the upper and bottom layers are set to be 600 μm and the heights of the control channels are set to be 100 μm so that the hydraulic drag caused by the surface tension effect can be neglected. The widths of the two crossed control channels (i.e., membrane length, L) are designed to be 100 μm, 200 μm, 300 μm or 400 μm, respectfully. After considering all the design parameters, it is concluded that the functional performances of the proposed regulator may be dependent on the W, H and L because these three parameters are directly related to the deformation area of membranes or the flow resistance of the regulator. For the sake of convenience, we use the symbol (W-L) H to refer to the type of empolyed devices in the following sections.

Device fabrication

The whole fabrication process of our passive flow regulator can be divided into the following four steps, as shown in Fig. 3a.

Lab on a Chip Accepted Manuscript

This journal is © The Royal Society of Chemistry 2012

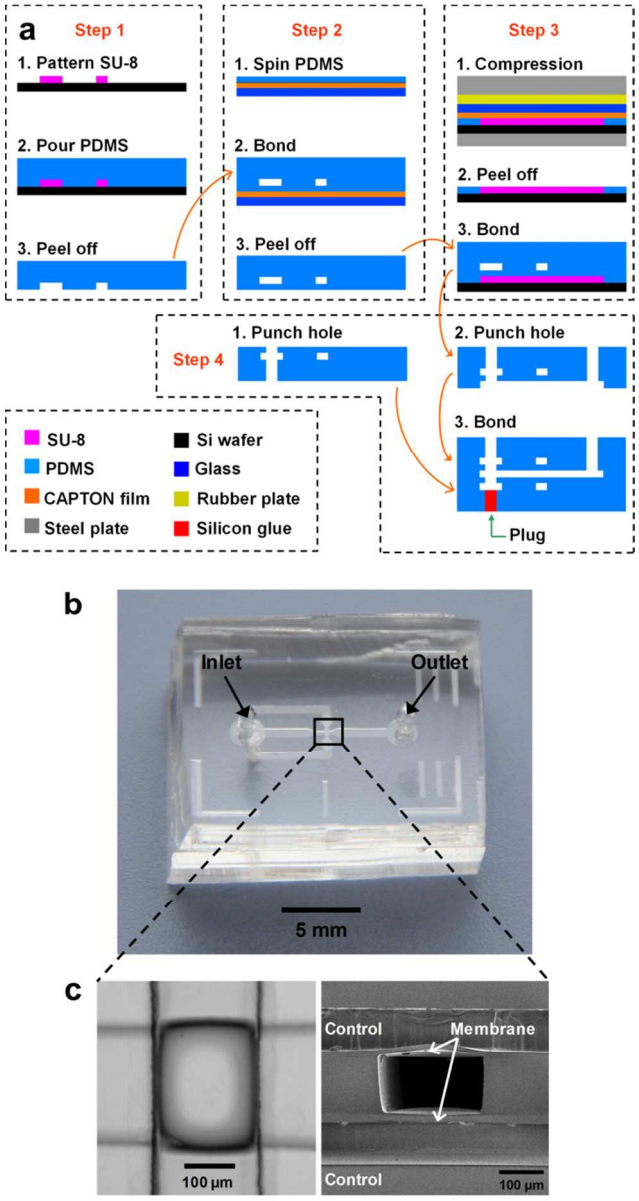

Fig. 3 Fabrication process and prototype device of our passive flow regulator: (a) Four-step fabrication process; (b) Photography of the fabricated device; (c) A microscope image of the observed membrane deflection under a pressure and a SEM picture of the cross-section of our regulator.

Step 1. The fabrication of control channel layers. This process step starts from the full-fledged photolithography for microchannel fabrication. Briefly, a layer of SU-8 2100 negative photoresist (MicroChem) with its thickness of 100 μm was patterned on the silicon wafer via the UV exposure to fabricate the master mold for PDMS micromolding. Then, mixed PDMS liquid (Slygard 184, Dow Corning, Base: Curing agent=10:1) was poured onto the prepared SU-8 master mold, and cured at 80 °C over 100 minutes in an oven. Finally, the cured PDMS replica was carefully peeled off from the master mold, obtaining the finished control channel layers for use in step 2.

Step 2. The fabrication and integration of membranes. The aim of this process step is to prepare an extremely thin PDMS membrane which can easily deform under external pressure forces. First, a thin CAPTON film was pasted onto the surface of a glass wafer for easy release of the fabricated membranes. Then, PDMS with a higher ratio of base to curing agent (20:1) was spun onto the CAPTON film to obtain a membrane of 10 μm thick. After curing, the membrane was bonded and integrated with the upper and bottom control channel layers with the assistance of the oxygen plasma treatment. Finally, the membrane together with the control channel layer was carefully peeled off from the CAPTON film, obtaining the upper and bottom covers for use in the following steps.

Step 3. The fabrication and assemble of the main channel layer. The aim of this process step is to fabricate an open channel layer with its thickness equal to the channel height. First, a master mold of 75 μm or 130 μm thick for replicating the main channel was fabricated in negative photoresist SU-8 2050 or SU-8 2150 using the photolithography technique. Then, the multilayer compression process was introduced to fabricate the open PDMS channel layer. The detailed process is summarized as follows.

a. PDMS (Base: Curing agent=10:1) was poured onto the fabricated SU-8 master mold of the main channel.
b. A CAPTON film was carefully lowered to the surface of the poured PDMS liquid. The surface tension between the film and the PDMS liquid would automatically pull the film to intimately contact with the PDMS, preventing the formation of bubbles at interfaces.
c. A glass wafer, a rubber plate and a heavy steel plate were placed onto the top of the CAPTON film one by one to extrude the excess uncured PDMS, which enables the thickness of the main channel layer be equal to that of the master mold.
d. The whole compression mold was then moved to the oven, and the PDMS was cured at 100 °C for 3 hours. After curing, a flat PDMS layer sticking into the SU-8 master mold was obtained. To prevent this thin PDMS layer from distorting, the middle main channel layer was aligned and bonded with the fabricated upper cover, forming a tight unit. In doing so, the main channel layer can be easily peeled off from the master mold together with the upper cover.

Step 4. Device final assemble. First, holes were punched at the bottom cover obtained from step 2 and the unit obtained from step 3, respectively. Then, deionized water was added to the oxygen plasma treated faces of the bottom cover and the unit as the surface lubricant to prevent from immediate bonding. Therefore, the two crossed control channels can be accurately aligned before bonding. Finally, the liquid silicon glue was employed to plug the hole in the bottom cover, obtaining the final prototype device, as shown in Fig. 3b. From the enlarged microscopic or SEM images (see Fig. 3c) of the fabricated device, it is validated that all these five separated layers are well bonded, and the two control channels in upper and bottom layers are well aligned to each other.

Flow-rate measurement experiments

In attempts to investigate the flow-rate characteristics of our passive flow regulator, a custom experimental setup was constructed, as shown in Fig. S1 in the Electronic Supplementary Information (ESI). In this experimental setup, condensed nitrogen gas was used as the power source for driving the sample fluids. The pressure of the flowing gas can be directly regulated via a handy pressure regulator, and monitored via a pressure sensor (Autonics, PSAN-C01CV-R_c1/8). An electronic balance (JM10002, Resolution 0.01g) was applied to measure the flow-rate of fluids flowing through the device via recording the mass increment in a certain time period. To understand the flow-rate characteristics of our regulator, we analysed

Lab on a Chip Accepted Manuscript

the influence of the critical parameters (i.e., L, W, and H) on delivery flow-rates of our regulator.

Influence of membrane length L on flow-rate

Four types of regulators (200-L)75 with different membrane lengths L and fixed cross-sectional dimensions (W=200 μm, and H=75 μm) were investigated. To make a contrast, we also fabricated and characterized a device (200)75 without membranes and control channels. The obtained relationship between the applied inlet pressure and the flow-rate is shown in Fig. 4a. From this figure, we found that with the increase of the inlet pressure, the flow-rates of the tested regulators increase gradually at first, and finally stabilize at a constant value, which perfectly validates the design function of our regulator. It is also noticed that the regulators with longer membrane lengths achieve relatively lower constant flow-rates, which means that the flow resistance of the regulator increases with the increase of membrane length. Specifically, the device (200-100)75 with a membrane length of 100 μm has a highest constant delivery flow-rate of 2.55±0.06 ml/min under the pressure of 25 kPa, while the device (200-400)75 obtains a lowest flow-rate of 1.12±0.05 ml/min under the pressure of 15 kPa. The threshold pressures of the tested four devices are all lower than 25 kPa and the variations of delivery flow-rates are calculated to be smaller than 5%, which shows a good competence of exporting a constant and predictable flow-rate. Comparatively, the experiment results of the simple channel device (200)75 show that the flow-rate increases proportionally to the inlet pressure because of the constant flow resistance.

Influence of cross-sectional dimension (WxH) on flow-rate

To study the influence of contraction gap width (W) on flow-rate, we compared the flow-rate characteristics of the devices (100-L)75 with that of devices (200-L)75. The membrane lengths L of these two device groups change from 200 μm to 400 μm, respectfully. Fig. 4b shows the experimental results of the tested regulators with different gap widths and membrane lengths. From this figure, we observed that all of the devices with a gap width of 100 μm achieve much lower constant flow-rates than that of devices with a gap width of 200 μm regardless of membrane lengths, which demonstrates that the decrease of gap width would result in a lower constant flow-rate. Similarly, we also compared the flow-rate characteristics of devices with different gap heights to understand the influence of cross-sectional heights (H) on flow-rate. The experimental results are illustrated in Fig. 4c, which shows that all the three types of devices (200-L)130 obtain higher constant flow-rates than devices (200-L)75, which indicates that increasing gap height would also increase the constant flow-rate. Therefore, it can be concluded from Fig. 4b and Fig. 4c that the constant flow-rates of devices are heavily dependent on cross-sectional dimensions, which means that increasing the cross-sectional area would decrease the flow resistance of the main channel, and thus increase the constant flow-rates of the regulators. Specifically, device (100-400)75 holds a lowest flow-rate of 0.86±0.04 ml/min, while device (200-200)130 obtains a highest flow-rate of 4.38±0.1 ml/min. All of the above-tested devices achieve the constant delivery flow-rates under the threshold pressures between 10 kPa and 20 kPa, and the calculated flow-rate variations are all smaller than 5%.

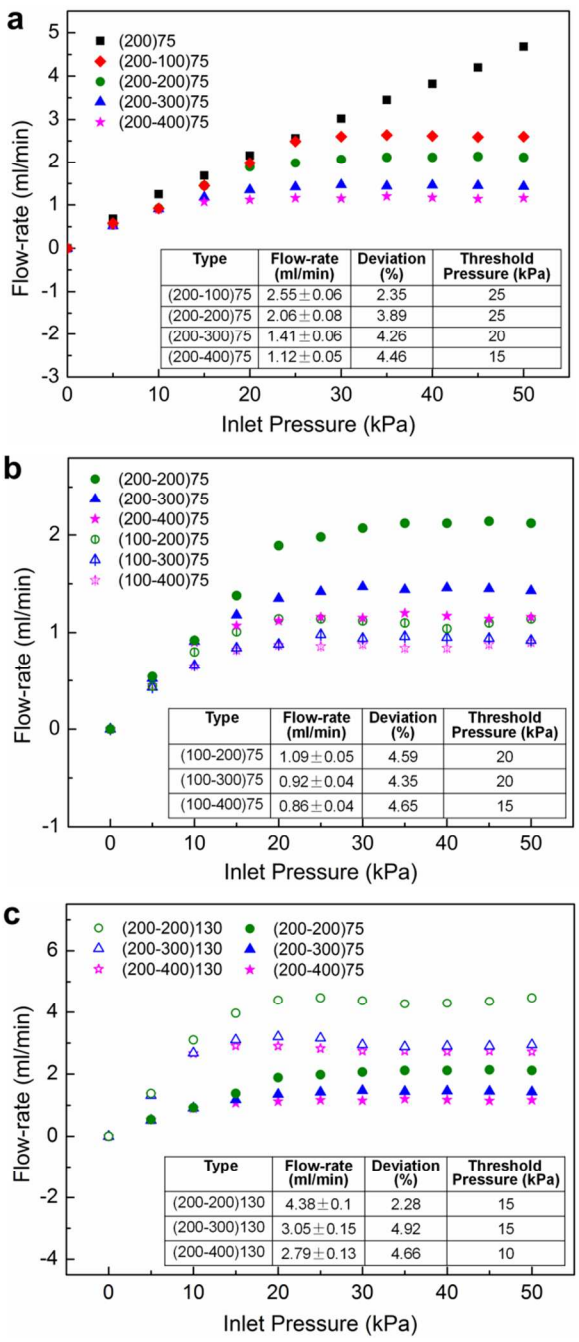

Type	Flow-rate (ml/min)	Deviation (%)	Threshold Pressure (kPa)
(200-100)75	2.55±0.06	2.35	25
(200-200)75	2.06±0.08	3.89	25
(200-300)75	1.41±0.06	4.26	20
(200-400)75	1.12±0.05	4.46	15

Type	Flow-rate (ml/min)	Deviation (%)	Threshold Pressure (kPa)
(100-200)75	1.09±0.05	4.59	20
(100-300)75	0.92±0.04	4.35	20
(100-400)75	0.86±0.04	4.65	15

Type	Flow-rate (ml/min)	Deviation (%)	Threshold Pressure (kPa)
(200-200)130	4.38±0.1	2.28	15
(200-300)130	3.05±0.15	4.92	15
(200-400)130	2.79±0.13	4.66	10

Fig. 4 Measured flow-rate characteristics of our passive flow regulator: (a) Influence of membrane length L on flow-rate; (b) Influence of contraction gap width W on flow-rate; (c) Influence of channel height H on flow-rate.

To embody the advantages of our regulator, we compared its functional performances with that of the recently reported state-of-the-art passive flow regulators[18-22]. The comparison results were listed in Table S1 (ESI), in which the performances of these regulators were compared in terms of the maximum constant delivery flow rate, operating pressure and flow-rate variation. As can be found from the comparison results, almost all the delivery flow rate of previously reported regulators are not qualified for high-throughput applications, especially such as inertial microbead isolation. The highest flow-rate achieved in the parallel membrane valve reported by Doh and Cho[21] is only 1.46±0.02 ml/min under a

Lab on a Chip Accepted Manuscript

 This journal is © The Royal Society of Chemistry 2012

relatively higher threshold pressure of 35 kPa. Although a feature of simple single-layer structure is offered by this reguator, a higher flow-rate can't be achieved because the required high aspect-ratio membrane is easy torn apart during the PDMS demolding process. By contrast, our regulator can achieve a much higher flow rate of 4.38±0.1 ml/min under a much lower threshold pressure of 15 kPa. The positive result confirms that our proposed passive flow regulator can realize the regulation of higher flow-rates under lower threshold inlet pressures. This unique feature would be very useful in low pressure driving microfluidics while high-throughput is still required.

Application validation experiments

Based on the above understandings, we applied our passive flow regulator for inertial isolation of microbeads. The inertial isolation is a newly emerging passive technique which employs the fluid inertia effects induced in finite Reynolds number flows[25], and thus has a unique advantage of high processing throughput over other microfluidic separation schemes[26,27]. In inertial isolation, the microbeads will be focused or dragged towards the certain lateral equilibrium regions, and then be isolated according to their different regions. However, the focusing statuses or positions of microbeads are found to be heavily dependent on the flow-rates, that is, the variation of flow-rate would significantly affect the inertial isolation performances. Therefore, the precise control of flow-rate is the key to success in applying inertial isolation for low-cost integrated microfluidic systems. Our regulator can fully meet the precise flow-rate control and high processing throughput requirements of inertial isolation. On the basis of our previous successful work on inertial microfluidics[28,29], we determined to choose the Dean Flow Fractionation (DFF) chip[30] as the detailed inertial isolation device. The DFF chip has two inlets and two outlets, and can isolate microbeads of two different diameters at an extremely high-throughput of ~ml/min level. However, due to the existence of two inlets and the usage of sheath flow, the flow in DFF chips is much more complex than other inertial microfluidic device, which raises an urgent demand for accurate flow controls.

Sample preparation, DFF chip design and pressure-flow characterization

Two polymer fluorescence microbeads (1% solids) with significantly different diameters (5 μm, Thermo Fisher Scientific, Inc. and 15 μm, Invitrogen) act as the sample microbeads for the following inertial isolation experiments. Here, we used deionized water to dilute the two concentrated microbead samples, obtainig a mixed suspension of 5 μm and 15 μm microbeads each accounting for 0.005% of the volume.

According to the determined isolation targets, we designed a DFF chip, as illustrated in Fig. 5a. The width of the spiral channel in this device was designed as 500 μm and its height was set to be 150 μm. The diameters of the inner and outer arcs of the spiral channel were set as 8.9 mm and 21.8 mm, respectively. The gaps between the adjacent spiral channels were designed to be 1 mm, and hence the total length of the spiral channel is approximately 120 mm. The 15 μm microbeads satisfy the focusing condition $a_p/h>0.07$[31] (where a_p and h denote the microbead diameter and the channel height, respectfully), and can be focused under the complex coupling of inertial lift force and Dean drag force while the smaller 5 μm microbeads would be in the mode of Dean migration due to the dominant Dean circulating effect. At a full Dean cycle (DC1), the 5 μm microbeads migrate towards the outer wall region and form a microbead band while the 15 μm microbeads focus near the inner wall, resulting in the separation of these two microbeads[30]. For achieving complete separation, the flow-rates of sheath flows and sample flows need to be carefully matched.

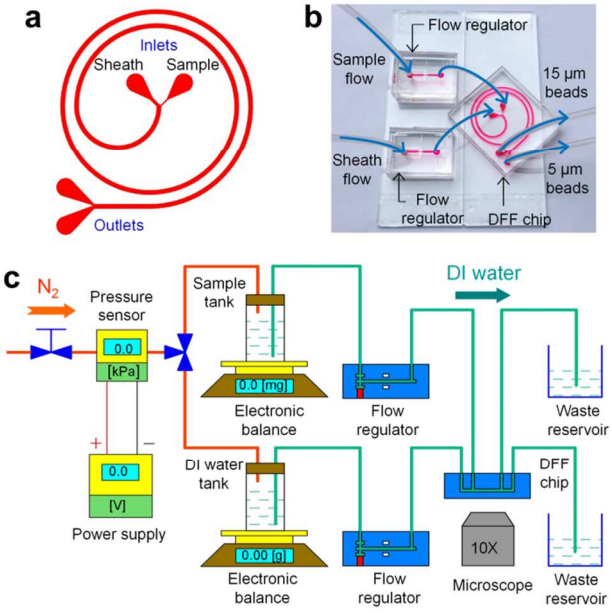

Fig. 5 Device characterization and gas-driven flow system: (a) Schematic diagram of the spiral channel in the DFF chip. (b) Photography of the flow control system integrated with two flow regulators and a DFF chip. The microchannels are filled with red dye for clear visualization. (c) Experimental setup of the gas-driven flow system.

To determine the available operation flow-rates for achieving microbeads isolation in the designed DFF chip, we first used two syringe pumps (LEGATO 270, KD Scientific) to provide constant sheath and sample flow-rates, and tested the available flow-rate range for microbead isolation achieved at a full Dean cycle (DC1). The measured flow-rate range for successful isolation is shown in Table S2 in ESI. From this experiment, we estimated that the available whole flow-rate range for microbead isolation is 0.9~1.25 ml/min. According to the Poiseuille's law[32], the calculated minimum differential pressure is approximately 27 kPa, which meets the requirement of threshold pressures (less than 50 kPa) for achieving a constant flow-rate in our regulators.

Gas-driven flow system construction

A gas-driven flow system was designed for inertial isolation of microbeads. In this system, we integrated two passive flow regulators to the sheath and sample flow inlets of the DFF chip (see Fig. 5b) for providing the constant sheath and sample flow-rates, respectfully. According the flow-rate range provided in Table S2, we chose the flow regulator (100-400)75 whose constant delivery flow-rate is 0.86 ml/min as the sheath flow regulator. Considering the relatively low flow-rate feature of the sample flow, we additionally fabricated a flow regulator (200-200)40 which holds a constant delivery flow-rate of 0.208±0.008 ml/min under a threshold pressure of 15 kPa as the sample flow regulator. Fig. 5c shows the schematic diagram of the gas-driven flow system for conducting the microbead isolation experiments. In this experimental setup, low pressure nitrogen gas was introduced as the power source for driving flows, and its pressure was real time monitored via a pressure sensor (Autonics, PSAN-C01CV-Rc1/8). Two electronic balances (JM10002, Resolution 0.01 g and CNSHP, FA2004, Resolution 0.01

Lab on a Chip Accepted Manuscript

mg) were used to measure the flow-rates of sheath flows and sample flows, respectively. An inverted fluorescence microscope (IX71, Olympus) was applied to observe the motion trajectories of the fluorescence microbeads flowing in spiral channels. The obtained experimental images were then captured using a 14-bit high-speed CCD (Retiga EXi, QImaging) and analysed through the IMAGE-PRO Express software (Media Cybernetics, Inc.).

Inertial isolation of microbeads

To validate the effectiveness of our flow regulator for precise inertial isolation under varied pressures, we first characterized the microbead isolation performances in the gas-driven flow system under different gas pressures of 25 kPa, 30 kPa, 40 kPa and 50 kPa. The stacked composite images illustrating the microbead distributions near the outlets are grouped in Fig. 6a (a video illustrating the real-time motions of microbeads is provided in video S1 in ESI). Both the composite images and the video confirm that the 5 μm and 15 μm microbeads achieve the continuously high-throughput isolation under varied pressures, and the average microbead-free gap between two microbead bands is measured to be stable at ~200 μm. Based on the above stacked images, a quantitative analysis of microbead distribution was carried out, as illustrated in Fig. 6b. The result indicates that the 15 μm microbeads focus near the inner wall region consistently, while the 5 μm microbeads form tight bands of constant widths totally independent of inlet pressure, which validate that our system is capable of accurate and stable flow control. To better understand the flow-rate characteristics in our flow control system, we further measured the sheath, sample and total Dean flow-rates under varied pressures from 10 kPa to 50 kPa. The experimental results are shown in Fig. 6c. From this figure, we observed that the sheath, sample and total Dean flow-rates both maintain to be constant when the gas pressure exceeds a threshold value of 25 kPa. As a comparison, we also characterized the microbead isolation performances in DFF chips without flow regulators, as illustrated in Fig.S2a in ESI. It is clearly shown that the isolation of these two microbeads can't be achieved under any applied pressure. Otherwise, without the constraint of flow regulators, the total Dean flow-rate increases proportionally to the inlet pressure (See Fig. S2b in ESI). Therefore, the integration of flow regulators overcomes the heavy dependence of flow-rate on isolation performances.

To further validate the isolation efficiency of our gas-driven flow system, we collected the isolated samples exported from the inner and the outer outlets under varied inlet pressures, and sampled the size distributions of collected two microbead samples under a microscope. The microscopic images in Fig. 6d validate that a 100%-complete isolation of these two microbeads was achieved. The extremely stable flow-rate offered by our flow control system makes it be suitable for various microfluidic applications required high-accurate flow control besides the microbead isolation. In addition, due to the low threshold pressure feature of our regulator, a lot of portable and low-cost apparatuses (e.g.,diaphragm pump or gas tank) can be used to drive the microfluidic flows.

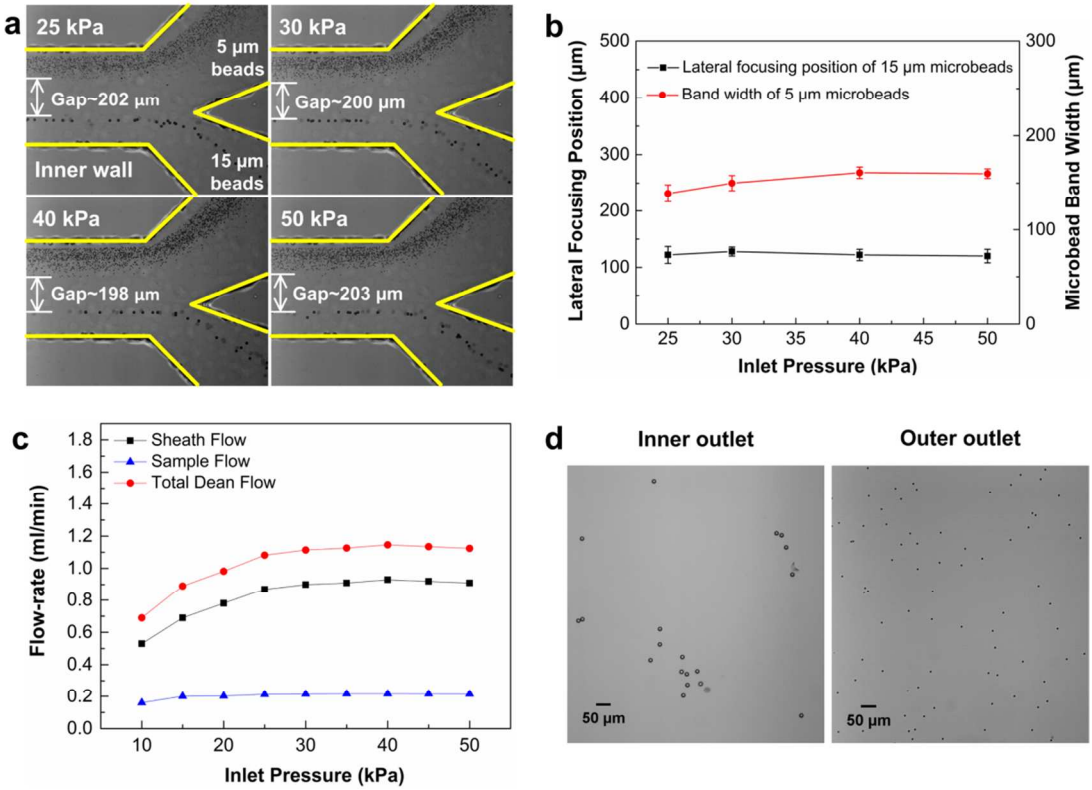

Fig. 6 Microbead isolation under varied gas pressures in the gas-driven flow system. (a) Composite images illustrating the distributions of microbeads near the outlet under varied pressures. (b) Quantitative analysis of microbead distribution under varied pressures. (c) Measured sheath, sample, and total Dean flow-rates as a function of inlet pressure. (d) The microscopic images of isolated microbeads collected from the inner outlet and the outer outlet.

Lab on a Chip Accepted Manuscript

This journal is © The Royal Society of Chemistry 2012

Conclusion

We designed and fabricated a series of five-layer-stacked PDMS passive flow regulators with different membrane lengths and cross-sectional dimensions. The fabricated prototype devices can realize the constant regulation of flow-rate up to 4.38±0.1 ml/min (the variation of flow-rate is smaller than 5%) while the minimum threshold pressure is only 10 kPa. These features are much better than that of previously reported regulators. To probe into the practical function of our passive flow regulator, we constructed an accurate and stable flow control system integrated with two passive flow regulators for both sample and sheath flows of a DFF chip to achieve high-throughput inertial isolation of two differently sized microbeads. The total flow-rate of the system is maintained to be constant when the gas pressure exceeds the threshold value of 25 kPa. In this system, isolation performance of microbeads is found to be totally independent of inlet pressure, and 100%-complete isolation of these two microbeads was achieved. In all, our passive flow regulator is potentially useful for many microfluidic fields where constant flow-rate is required. The low threshold pressure feature offered by our regulator enables various portable and low-cost apparatuses (e.g., diaphragm pump or gas tank) be used for driving microfluidic flows.

Acknowledgements

This work was supported by the National Natural Science Foundation of China (51375089), the National Basic Research Program of China (2011CB707601) and the Specialized Research Fund for the Doctoral Program of Higher Education (20110092110003).

Notes and references

[a]School of Mechanical Engineering, and Jiangsu Key Laboratory for Design and Fabricate of Micro-Nano Biomedical Instruments, Southeast University, Nanjing 211189, China
§These authors contributed equally to this work
*Corresponding author: nzh2003@seu.edu.cn
†Electronic Supplementary Information (ESI) available: Further information about the comparison of the passive flow regulators, measured flow-rates for microbead isolation, experimental setup for flow-rate measurement, the isolation performance of microbeads without regulators, and a video illustrating the real-time motions of microbeads can be found in the ESI. See DOI: 10.1039/b000000x/

1 K. W. Bong, S. C. Chapin, D. C. Pregibon, D. Baah, T. M. F.-Smith and P. S. Doyle, *Lab Chip*, 2011, **11**, 743-747.
2 Y. J. Kang and S. Yang, *Lab chip*, 2012, **12**, 1881-1889.
3 K. Iwai, R. D. Sochol and L. Lin, *MEMS 2011,* Cancun, MEXICO (Jan. 23-27, 2011), pp. 1131-1134.
4 M. A. Unger, H. P. Chou, T. Thorsen, A. Scherer and S. R. Quake, *Science*, 2000, **288**, 113-116.
5 X. Y. Peng, *Lab chip*, 2011, **11**, 132-138.
6 D. Anjewierden, G. A. Liddiard and B. K. Gale, *J. Micromech. Microeng.,* 2012, **22**, 025019.
7 H. Chen, J. Cogswell, C. Anagnostopoulos and M. Faghri, *Lab chip*, 2012, **12**, 2909-2913.
8 J. Goldowsky and H. F. Knapp, *RSC Adv.*, 2013, **3**, 17968-17976.
9 R. Safavieh and D. Juncker, *Lab chip*, 2013, **13**, 4180-4189.
10 B. Ziaie, A. Baldi, M. Lei, Y. Gu and R. A. Siegel, *Adv. Drug Delivery Rev.*, 2004, **56**, 145-172.
11 R. Sista, Z. Hua, P. Thwar, A. Sudarsan, V. Srinivasan, A. Eckhardt, M. Pollack and V. Pamula, *Lab Chip*, 2008, **8**, 2091-2104.
12 N. M. Karabacak, P. S. Spuhler, F. Fachin, E. J. Lim, V. Pai, E. Ozkumur, J. M. Martel, N. Kojic, K. Smith, P.-i Chen, J. yang, H. Hwang, B. Morgan, J. Trautwein, T. A. Barber, S. L. Stott, S. Maheswaran, R. Kapur, D. A. Haber and M. Toner, *Nat. Protoc.*, 2014, **9**, 694-710.
13 A. R. Abate and D. A. Weitz, *Appl. Phys. Lett.*, 2008, **92**, 243509.
14 V. Bazargan and B. Stoeber, *J. Microelectromech. Syst.*, 2010, **19**, 1079-1087.
15 S. Matsumoto and Y.-C. Tai, *JSME Int. J., Ser. B*, 2004, **47**, 528-533.
16 A. R. Abate, J. J. Agresti and D. A. Weitz, *Appl. Phys. Lett.,* 2010, **96**, 203509.
17 H. Kim and J. Kim, *Microfluid. Nanofluid.*, 2014, **16**, 623-633.
18 P. Cousseau, R. Hirschi, B. Frehner, S. Gamper and D. Maillefer, *Proceeding of the 14th IEEE International Conference on Micro Electro Mechanical Systems (MEMS 2001)*, Interlaken, Switzerland (Jan. 21-25, 2001), pp. 527-530.
19 E. P. Kartalov, C. Walker, C. R. Taylor, W. F. Aderson and A. Scherer, *Proc. Natl. Acad. Sci. U. S. A.*, 2006, **103**, 12280-12284.
20 H.-J Chang, W. Ye and E. P. Kartalov, *Lab chip*, 2012, **12**, 1890-1896.
21 I. Doh and Y.-H Cho, *Lab chip*, 2009, **9**, 2070-2075.
22 B. Yang and Q. Lin, *J. Microelectromech. Syst.,* 2007, **16**, 411-419.
23 I. Doh and Y.-H Cho, *Proceedings of PowerMEMS 2008+ microEMS 2008*, Sendai, Janpan (Nov. 9-12, 2008), pp. 89-92.
24 A. Debray, T. Nakakubo, K. Ueda, S. Mogi, M. Shibata and H. Fujita, *The Fourth International Workshop on Micro and Nanotechnology for Power Generation and Energy Conversion Applications(PowerMEMS 2004)*, Kyoto, Japan (Nov. 28-30, 2004), pp. 42-45.
25 D. D. Carlo, *Lab chip*, 2009, **9**, 3038-3046.
26 J. M. Martel and M. Toner, *Annu. Rev. Biomed. Eng.*, 2014, **16**, 371-396.
27 H. Amini, W. Lee and D. D. Carlo, *Lab chip*, 2014, **14**, 2739-2761.
28 N. Xiang, H. Yi, K. Chen, D. Sun, D. Jiang, Q. Dai, and Z. Ni, *Biomicrofluidics*, 2013, **7**, 044116.
29 N. Xiang, K. Chen, D. Sun, S. Wang, H. Yi, and Z. Ni, *Microfluid. Nanofluid.*, 2013, **14**, 89-99.
30 H. W. Hou, M. E. Warkiani, B. L. khoo, Z. R. Li, R. A. Soo, D. S.-W Tan, W.-T Lim, J. Han, A. A. S. Bhagat and C. T. Lim, *Sci. Rep.*, 2013, **3**, 1259.
31 D. D. Carlo, D. Irimia, R. G. Tompkins and M. Toner, *Proc. Natl. Acad. Sci. U. S. A.*, 2007, **104**, 18892-18897.
32 F. M. White, *Viscous Fluid Flow*, New York, McGraw-Hill, 2nd edn, 1991, 114-132.

Lab on a Chip Accepted Manuscript